High resolution AFM studies of irradiated mica-following the traces of swift heavy ions under grazing incidence

E. Gruber, L. Bergen, P. Salou, E. Lattouf, C. Grygiel, Y. Wang, A. Benyagoub, D. Levavasseur, J. Rangama, H. Lebius, et al.

HAL Id: hal-02393741

https://hal.science/hal-02393741

Submitted on 4 Dec 2019

PAPER • OPEN ACCESS

High resolution AFM studies of irradiated mica—following the traces of swift heavy ions under grazing incidence

To cite this article: Elisabeth Gruber *et al* 2018 *J. Phys.: Condens. Matter* **30** 285001

View the article online for updates and enhancements.

Related content

IOP ebooks™

Bringing you innovative digital publishing with leading voices to create your essential collection of books in STEM research.

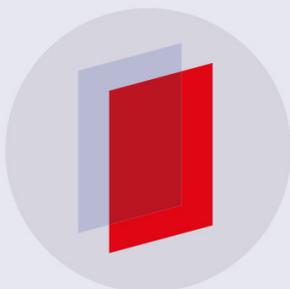Start exploring the collection - download the first chapter of every title for free.

High resolution AFM studies of irradiated mica—following the traces of swift heavy ions under grazing incidence

Elisabeth Gruber[1,5] , **Lorenz Bergen**[1]**, Pierre Salou**[2]**, Elie Lattouf**[2]**, Clara Grygiel**[2]**, Yuyu Wang**[4]**, Abdenacer Benyagoub**[2]**, Delphine Levavasseur**[2]**, Jimmy Rangama**[2]**, Henning Lebius**[2] **, Brigitte Ban-d'Etat**[2]**, Marika Schleberger**[3] **and Friedrich Aumayr**[1]

[1] TU Wien, Institute of Applied Physics, 1040 Vienna, Austria
[2] CIMAP (CEA-CNRS-ENSICAEN-UCN), Blvd. Henri Becquerel, 14070 Caen Cedex 5, France
[3] Universität Duisburg-Essen, Fakultät für Physik and Cenide, 47057 Duisburg, Germany
[4] Chinese Academy of Sciences, Institute of Modern Physics, 730000 Lanzhou, People's Republic of China

E-mail: elisabeth.gruber@phys.au.dk

CrossMark

Abstract

High resolution AFM imaging of swift heavy ion irradiated muscovite mica under grazing incidence provides detailed insight into the created nanostructure features. Swift heavy ions under grazing incidence form a complex track structure along the surface, which consists of a double track of nanohillocks at the impact site accompanied by a single, several 100 nm long protrusion. Detailed track studies by varying the irradiation parameters, i.e. the angle of incidence (0.2°–2°) and the kinetic energy of the impinging ions (23, 55, 75, 95 MeV) are presented. Moreover, the track formation in dependence of the sample temperature (between room temperature and 600 °C) and of the chemical composition (muscovite mica and fluorphlogopite mica) is studied.

Keywords: swift heavy ions, muscovite mica, high resolution AFM, ion tracks, grazing incidence, nanostructure formation

(Some figures may appear in colour only in the online journal)

1. Introduction

An intriguing phenomenon in ion-surface interaction is the formation of nanostructures due to single ion impact. Besides the interest in understanding the underlying physical mechanisms, this research field is driven by the interest of using ions as a tool for lithographic modifications. Investigations of various materials have shown that irradiations with swift heavy ions (SHI) induce severe structural modifications at the surface and in the bulk [1–4]. These modifications appear as protrusions or craters on the surface, show up as phase transitions (e.g. from crystalline to amorphous) and/or create latent tracks of several hundreds of nanometer into the solid. The formation of tracks and surface nanostructures occurs predominantly in insulators (e.g. polymers [5], oxides [6], ionic crystals [3, 7]) and is linked to a critical (electronic) energy loss dE/dx of the projectile [8].

Besides studies of track formations created under perpendicular incidence, the nanostructures produced under grazing incidence have attracted increasing interest due to the observation of novel nanoscale features. These new features include a chain-like morphology of ion tracks [6], groove formation in

[5] Present address: Aarhus University, Department of Physics and Astronomy, 8000 Aarhus C, Denmark
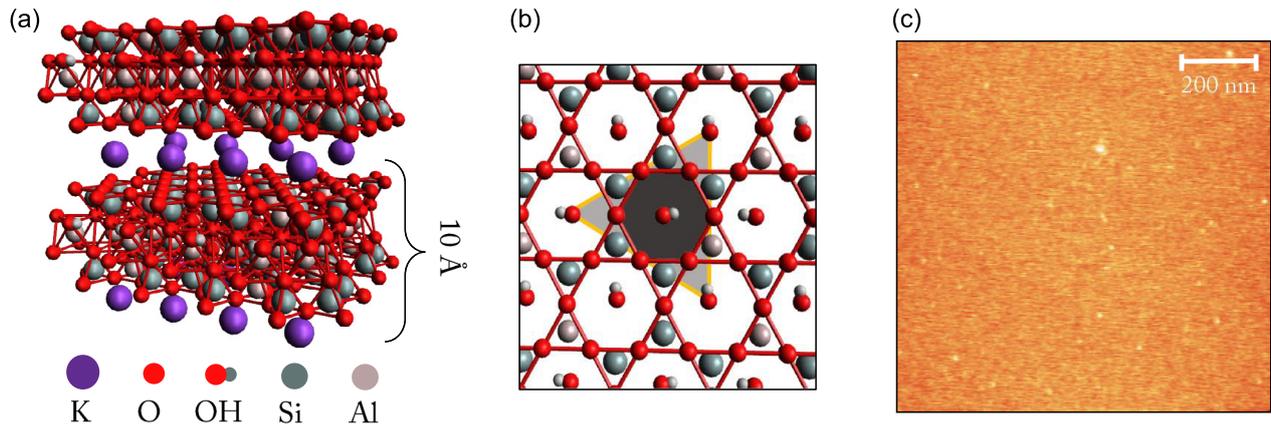
Figure 1. (a) The crystalline structure of muscovite mica consists of negatively charged alumino-silicate layers with intermediate layers of positive potassium ions to provide charge neutrality. The layered structure enables an easy cleaving of the crystal providing smooth and atomically flat surfaces. (b) Top view of the crystal. (c) Topography of an unirradiated mica sample with a RMS-roughness value of 0.07 nm, obtained by ambient AFM imaging in tapping mode.
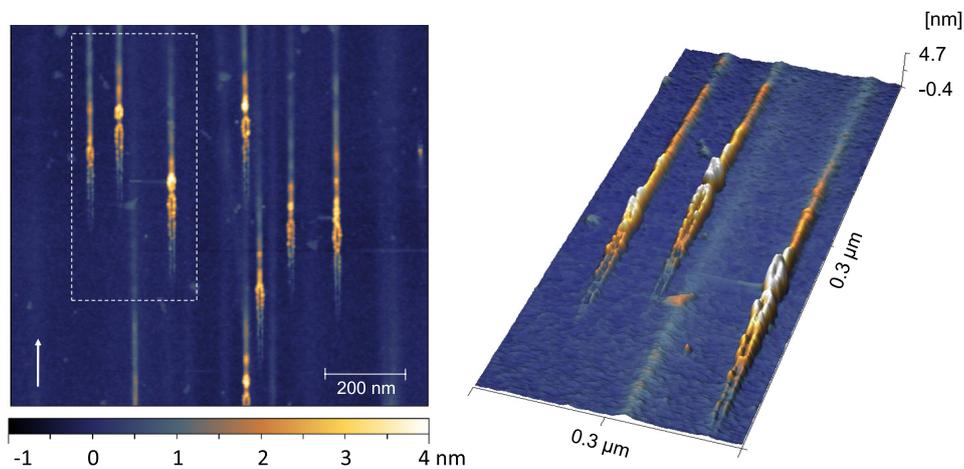

Figure 2. AFM images of a mica surface after irradiation with 92 MeV ^{129}Xe^{23+} ions under a grazing incidence angle of 0.7°. The 3D image represents the highlighted area. The formation of a double track at the impact site which merges into a high hillock, followed by a decreasing protrusion, can be observed.

3D [9] and 2D materials [10], creation of nanoholes within ion tracks [11], cratering in polymers [5, 12], formation of conductive ion tracks [13] and folding and unzipping of graphene deposited on a substrate [14–16]. Recently we could show that SHI irradiation of CaF$_2$ leads to a complex track formation consisting of a long groove bordered by chains of equally spaced nanodots eventually followed by a single chain of unseparated nanodots with a single high hillock at the beginning [17].

Within a palette of various materials, mica is an ideal candidate to study ion induced surface modifications because of its radiation sensitivity and easy preparation of nearly perfect surfaces (see figure 1). It belongs to the sheet silicate minerals and includes several closely related materials with a monoclinic crystal system. The most prominent candidate is thereby muscovite mica with the sum formula KAl$_2$[AlSi$_3$O$_{10}$(OH)$_2$]. It consists of negatively charged alumino-silicate layers, involving both tetrahedral and octahedral sheets, with intermediate layers of positive potassium ions to provide charge neutrality [18]. The layered structure of mica makes an easy cleaving of the crystal possible, providing smooth and atomically flat surfaces.

Earlier AFM investigations of SHI irradiated mica samples under perpendicular incidence have shown the appearance of hollows or hillocks in dependence of the direction of the cantilever movement. This artificial topographic features were explained by frictional forces [19] and changes of the elastic properties due to SHI irradiations [20]. Lateral force mode measurements could also show an increase of the track diameters with an increase of the energy loss [21]. The situation changes by using particles with similar energy loss values (some tens of keV nm^{-1}) but much lower kinetic energies (some MeV in comparison to GeV). In this case the formation of true topographic hillocks were reported [22]. True topographic features could also be observed by Daya *et al* [23–25] after irradiation with 78.2 MeV ^{127}I ions or with 20.4 MeV C$_{60}$ clusters. While for 78.2 MeV ^{127}I irradiation hillocks with a height of about 0.5 nm were created, 'gigantic' (nearly seven times taller and two times broader) conical hillocks were observed after 20.4 MeV C$_{60}$ irradiations. These differences were explained by the much higher total stopping power (3.6 times higher) of C$_{60}$ in comparison to 78.2 MeV ^{127}I.
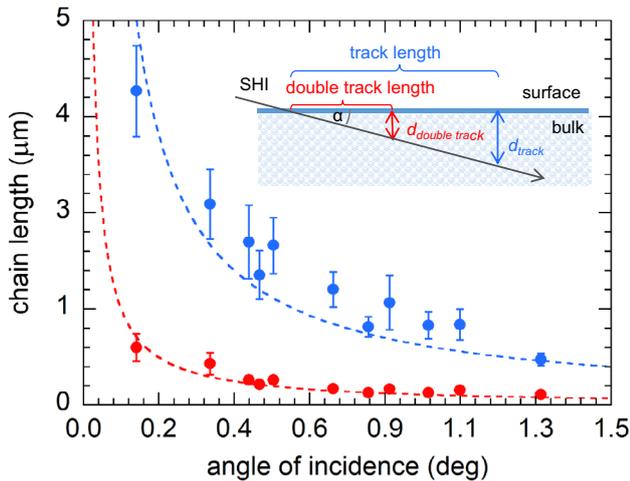
Figure 3. Evaluation of the double track length and the whole protrusion length in dependence of the incidence angle. The data points are fitted by the relation $L = d/\tan(\alpha)$ and a value of $d_{\text{double track}} = 2.3$ nm and $d_{\text{track}} = 13$ nm is extracted. The inset shows a schematic of the geometrical considerations.

First SHI irradiations under grazing angle of incidence revealed the creation of conical shaped hillocks accompanied by raised tails [23]. At closer look also the formation of topographical craters next to each hillock could be observed [25]. From these first images further details of the nanofeatures are hard to identify due to the limited image quality and insufficient spatial resolution. Blunt tip ends result in a complete masking of the crater and a broad and blobby image of the hillocks.

In this paper we present high resolution AFM studies of muscovite mica irradiated with SHI under grazing incidence. Detailed AFM investigations are presented which show that the nanostructure features of the created track structures are as complex as the observed tracks on CaF_2 [17]. Moreover, studies of the track formation in dependence of the projectile kinetic energy, the sample temperature and the sample chemical composition are presented.

2. Experimental methods

Irradiations of the mica samples were carried out at the IRRSUD facility of GANIL (Grand Accelerateur National d'Ions Lourds) in Caen, France. Freshly cleaved mica samples, which were obtained by placing a piece of tape onto the mica surface and gently pulling off the first layers, have been irradiated during several measurement periods with $^{136}Xe^{23+}$, $^{129}Xe^{23+}$ and $^{208}Pb^{29+}$ ions at kinetic energies of 0.71 MeV amu^{-1} and 0.48 MeV amu^{-1}, respectively. To perform irradiations also at lower kinetic energies, Al foils of different thickness (1.5, 3 and 6 μm) were inserted into the beam to act as energy degraders. The targets were mounted on a vertical target holder, which could be rotated around the vertical axis by a stepping motor with a repeatability of about 5/100 of a degree. The angle of incidence, measured with respect to the surface plane, was varied between 0.2° and 2°. An ion fluence between 1×10^{10} ions cm^{-2} and 5×10^{10} ions cm^{-2}, depending on the incident angle, was chosen, to avoid overlapping of the created

ion tracks. The samples were inspected immediately after irradiation with a VEECO NanoScope III atomic force microscope in Caen and detailed AFM investigations were performed with the Asylum Research Cypher Scanning Probe Microscope at TU Wien. The AFM measurements were performed in tapping mode under ambient conditions with standard Si cantilevers OMCL-AC240TS-R3 (Olympus) with a typical tip radius of curvature of 7 nm, a resonance frequency of 70 kHz and a spring constant of 1.7 N m^{-1}. Further data evaluation has been performed with the software Gwyddion [26].

3. Experimental results and discussion

3.1. Surface topography of irradiated mica-high resolution AFM imaging

At first sight, the irradiation of muscovite mica under grazing incidence leads to the formation of long tracks which consist of a chain of single nanodots at the impact site followed by a long sloping protrusion. Remarkable for the irradiated mica samples are the extraordinary long tracks formed along the surface. At small incidence angle of ~0.2° tracks of several hundreds of nm in length are formed. By performing high resolution AFM imaging much more details of the created nanostructure features can be identified. The 2D and 3D AFM images of figure 2 show the typical topography of a muscovite mica surface after SHI irradiation under grazing angle of incidence of 0.7°. The white arrow indicates the direction of the incoming ions. Individual ion impacts create parallel arranged tracks whose structure appears as complex as that found recently for CaF_2 [17]. At the impact site a double track is formed consisting of two parallel arranged chains of single nanodots whose height increases up to about 5 nm before merging into a single protrusion that fades at large distance. The distance D between the two hillock rows of the double track is only 10 nm and the finite radius of curvature of the used tip may prevent an observation of a shallow groove in between them.

The length of the double track and the length of the whole protrusion can be controlled by varying the angle of incidence [27]. In figure 3 the length of the double track and of the whole track is plotted as a function of the incidence angle α and follows the relation $L = d/\tan(\alpha)$. We determined the (double) track length as a function of the angle of incidence by analyzing at least 50 tracks for each angle. This relation was also previously observed for other materials [6, 9, 17] and is motivated by simple geometrical considerations, where L is the (double) track length and d the maximum depth from which this particular ion induced modification can still be detected at the surface. The fitting parameter d gives indication about the radius of the modified track and how far the local excitation is spread. It is characteristic for a certain material. The fit yields a characteristic depth of $d_{\text{double track}} = 2.3$ nm for the double track features and $d_{\text{track}} = 13$ nm for the whole track formation. The length d_{track} evaluated for mica is about twice as long as observed for other dielectric materials [28]. It shows the high radiation sensitivity of mica.
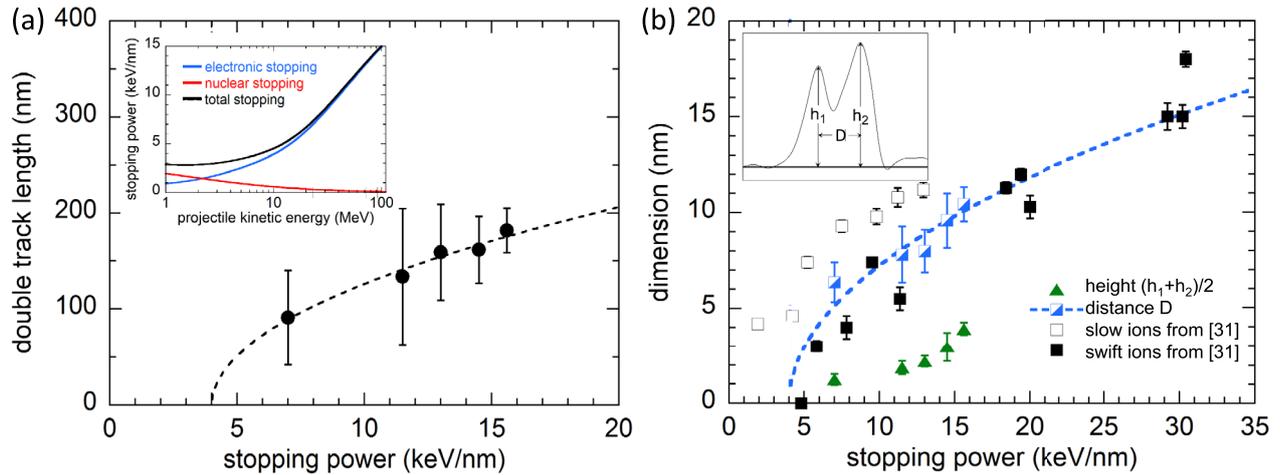
Figure 4. (a) The figure shows the evaluated double track length as a function of the stopping power. The stopping power was calculated by using the SRIM code for a Xe atom impacting on mica with a density of $\rho = 2.82$ g cm^{-3} (see inset). The dashed line represents a square root fit through the data points and gives a threshold value of ~ 4 keV nm^{-1}. (b) The figure shows the distance D between opposite lying hillocks of the double track and the height of the hillocks of the double track in dependence of the stopping power. The inset illustrates what is meant by the distance and the mean value of the height. For comparison track diameters created by slow $E < 0.6$ MeV amu^{-1} and swift $E > 4.8$ MeV amu^{-1} ions (taken from [31]) are shown. The data can be fitted by a square root function which is done exemplary for our data (dashed line) by assuming a threshold value of 4 keV nm^{-1}, obtained from figure 4(a). An increase of the hillock height with an increase of the stopping power can be observed.

3.2. Variation of the ion kinetic energy

The track formation and nanostructure creation efficiency depend strongly on the density of energy released to the electronic system near the ion path. The density of electronic excitation is generally characterized by the electronic stopping $\mathrm{d}E/\mathrm{d}x$. For track formation the amount of deposited energy as well as the spatial deposition of the released energy play an important role. While the irradiation with projectiles at high kinetic energies leads indeed to higher stopping power up to the maximum of the energy loss curve, the damage cross section is larger for ions at low velocity than at high velocity. For low-velocity ion projectiles the transferred energy to the primary electrons is reduced and accordingly the electron cascade is less extended. The deposited energy is kept within a shorter distance around the ion path, the ionization density is increased and the resulting damage formation is enhanced (velocity effect) [29]. Since the cross section is linear with the stopping power $S = \mathrm{d}E/\mathrm{d}x$, the track radius, which is equal to the square root of the cross section divided by π, follows the square root of the electronic stopping [8].

We performed ion irradiations by varying the incident kinetic energy between 0.17 and 0.71 MeV amu^{-1} and evaluated the double track length as a function of the stopping power (see figure 4(a)). The stopping power was calculated by using the SRIM code [30] for a Xe atom at $E_{\mathrm{kin}} = 23, 52, 72$ and 92 MeV impacting on mica with a density of $\rho = 2.82$ g cm^{-3}. The evaluated data for the double track length are fitted by the relation $L = k \cdot \sqrt{S - S_{\mathrm{threshold}}}$ which yields a threshold value of $S_{\mathrm{threshold}} \sim 4$ keV nm^{-1}, comparable to earlier predicted threshold values for mica [20, 31].

Besides the length of the double track, the width and the height of the hillocks of the double track were also evaluated in dependence of the stopping power. Both show an increase for higher stopping power (see figure 4(b)). To exclude an

overestimation of the width of the double track due to the convolution of the tip and the nanostructure features, the distance D between opposite lying hillocks was chosen as a reliable measure (see inset of figure 4(b)). In figure 4(b) the evaluated data for the distance D are compared with the evaluated track radii from the literature [31]. Therein, the track diameter for slow ($E < 0.6$ MeV amu^{-1}) and swift ($E > 4.8$ MeV amu^{-1}) ions were determined by using an atomic force microscope under air in contact mode. Our data, obtained for $E < 0.7$ MeV amu^{-1} are in good agreement with these data, keeping in mind that our data represent the distance D between the hillock chains of the double track and may thereby underestimate the real track diameter. The data were fitted again by a square root function, by assuming a threshold value of 4 keV nm^{-1} obtained from the fit in figure 4(a).

3.3. Track formation studies in dependence of the sample temperature

The track size may not only depend on the projectile velocity but also on the sample temperature. For SHI irradiation of Bi, for example, it was shown that the track size changes drastically by performing irradiations between 20 and 300 K [8]. The irradiation of samples and yet the deposition of energy into the system leads to a temperature rise which eventually induces melting or sublimation of the target material [17]. A variation of the sample temperature may thus change the threshold above which projectile induced damage becomes visible or may change the nanostructure features of the created tracks. We therefore heated the mica samples at 200 °C, 400 °C or 600 °C during irradiation and performed AFM studies to investigate possible effects on the track formation. A heating of the mica samples to 600 °C or above has to be avoided, since at these higher temperatures the surface
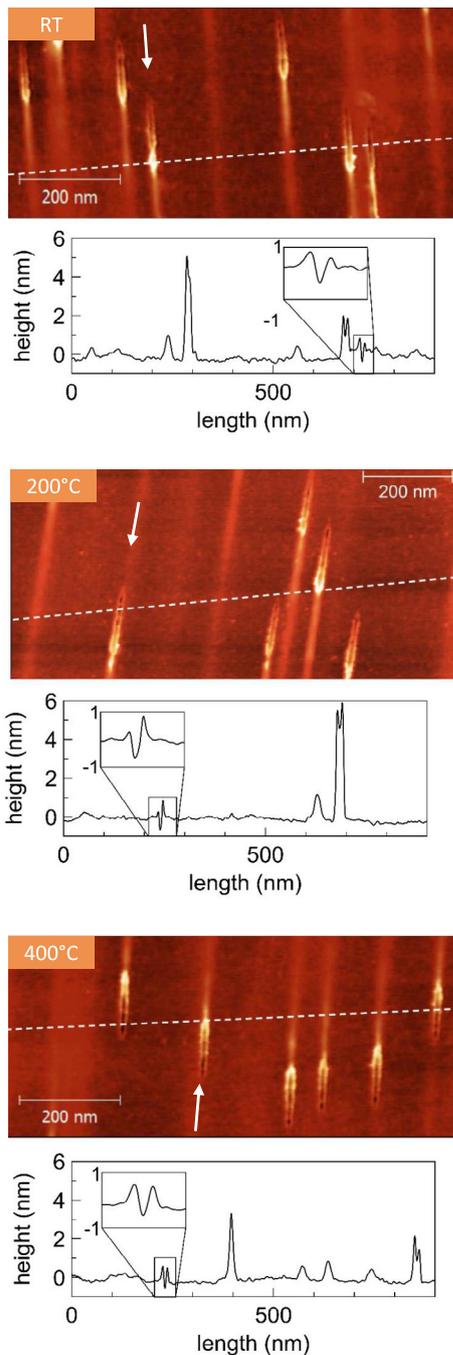
Figure 5. Track formations on mica due to $^{208}Pb^{29+}$ ion impacts at room temperature at 200 °C and at 400 °C. The dashed lines in the images indicate where the line profiles, shown below, are taken from. All three images show the formation of a double track at the impact site (zoomed figures), the merging of the double track into a huge ~5–6 nm high single hillock, followed by a decreasing protrusion with a height of ~1–2 nm.

becomes cracked [32, 33, 34] and makes investigations of surface modifications due to single ion impacts inaccessible.

In figure 5 the topography of an irradiated unheated mica sample is compared with irradiated samples heated at 200 °C and 400 °C. For all three samples the profiles through the created tracks show the formation of a double track at the impact site which merges into a single protrusion with a ~5 nm high

hillock at its beginning. The nanostructure features of the created tracks seem to be unaffected by the sample temperature (figure 6). Only a slight increase of the track length for the heated samples is apparent (figure 6(a)) and in the case of the 400 °C heated sample (figure 5) the formation of the groove between the double track is more pronounced. A further increase of the sample temperature and thus an approach of the melting temperature of mica was not possible due to the above mentioned destruction of the mica surface.

3.4. Track formation studies in dependence of the chemical composition of mica

A more pronounced groove formation between the double track at the impact site could be observed by performing irradiation at room temperature with fluorphlogopite mica $KMg_3(AlSi_3O_{10})F_2$. In this synthetic mica the $(OH)^-$ group is fully substituted by F^- ions. Samples of this chemical composition are characterised by superior thermal stability. They can be used up to 1100 °C with almost no changes and will decompose gradually only at 1200 °C. Muscovite mica with the $(OH)^-$ group begins to decompose already above 450 °C and is almost completely decomposing at 900 °C. The melting temperature of muscovite mica lies between 700 and 1000 °C, whereas in the case of fluorphlogopite mica it is at about 1350 °C. A comparison of AFM images of muscovite mica and fluorphlogopite mica after irradiation under the same conditions shows on both samples parallel arranged tracks with slightly different topographical characteristics. For muscovite mica the formation of a double track consisting of single nanodots and a possible cavity in between is formed. However, in the case of fluorphlogopite mica a long ditch with no bordered nanodots is notable (figure 7(a)). The first nanodots appear much later in the modification. In both cases the double track eventually merges into a long decaying protrusion. The tracks on fluorphlogopite mica are slightly longer than those obtained on muscovite mica (figure 7(b)) and the created grooves are more pronounced. Moreover the height of the protrusion is on average only a third of the value obtained with muscovite mica (compare figures 6(b) and 7(c)). Recent etching investigations of mica [35] have shown that the track etch rate in muscovite mica is low in comparison to phlogopite mica because of the greater Al-O bond strength. The weaker bond strength in the case of fluorphlogopite mica may also explain the more pronounced and effective groove formation after SHI irradiation.

In the case of fluorphlogopite mica the formation of grooves at the impact site is clearly visible and the groove volume can be estimated. For the samples irradiated under grazing incidence of 1.4° a groove volume of ~120 nm³ at a length of 110 nm is estimated. For the samples irradiated under 1° a volume of ~220 nm³ at a length of 235 nm is evaluated. By assuming a particle density of $n_{at} \sim 8 \cdot 10^{22}$ atoms cm^{-3} this yields a number of ~9 · 10³ and ~19 · 10³ missing atoms, respectively. Since the grooves are not bordered by nanodots and the first protrusions appear much later in the modification, it might be reasonably assumed that the missing atoms have left the surface. In order to check whether the particle
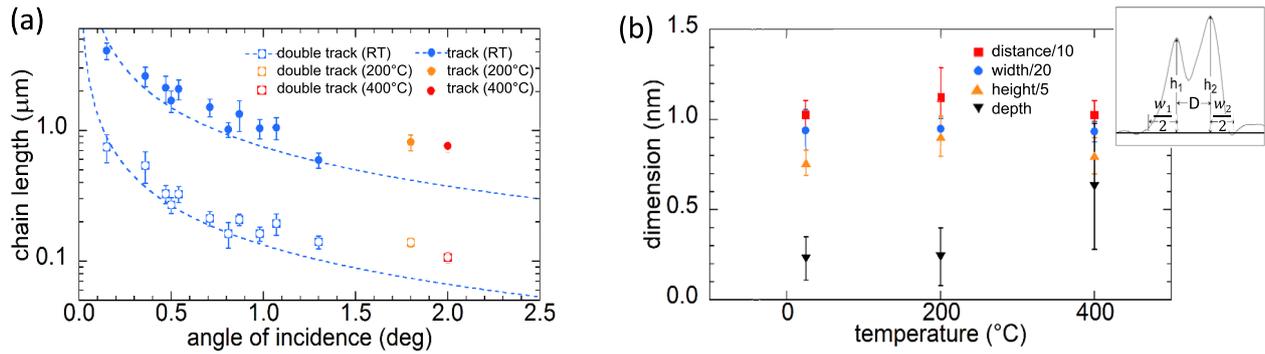
Figure 6. (a) The double track and whole track lengths for the heated samples are compared with the results obtained from the unheated samples. A slight increase of the lengths for the heated mica samples can be observed. In (b) the mean distance D between the hillock rows, the mean width $(w_1 + w_2)/2$ of single hillocks, the mean height $(h_1 + h_2)/2$ of single hillocks and the depth of the formed grooves are plotted for the unheated and heated mica samples. For better readability the values are rescaled by the given factor in the label.
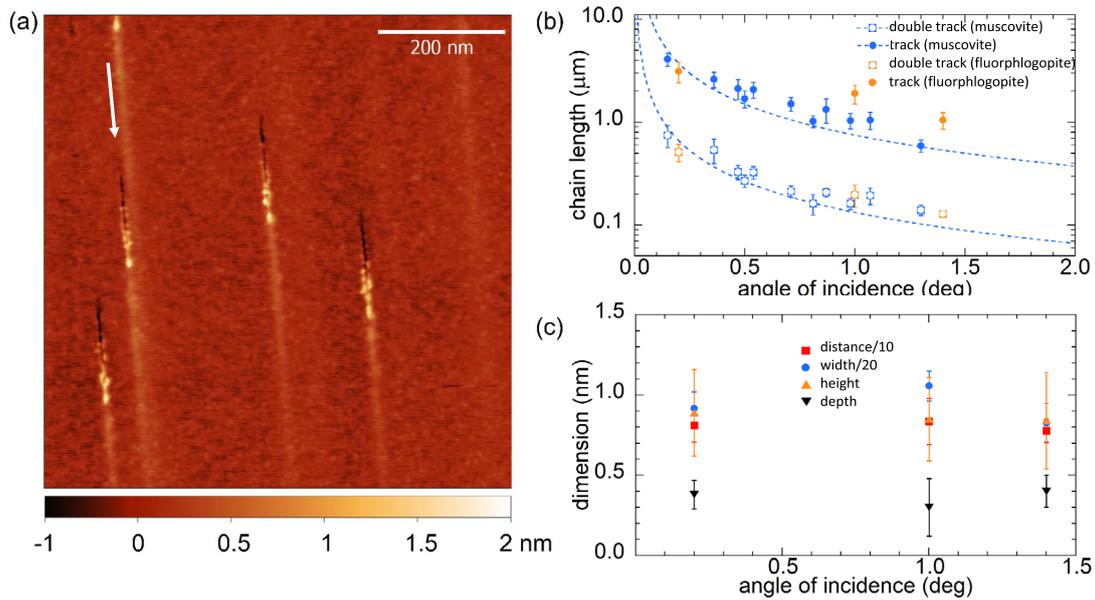

Figure 7. (a) AFM image of fluorphlogopite mica irradiated with $^{129}Xe^{23+}$ under grazing angle of incidence of 1.4°. The irradiation was performed at room temperature. The formation of a long ditch, followed by chains of nanodots and a long decaying protrusion, can be observed. (b) Evaluation of the double track/groove and track lengths created on fluorphlogopite mica in comparison to muscovite mica. (c) Parameters of the double track/groove of irradiated fluorphlogopite mica. For better readability the values are rescaled by the given factor in the label.

deposited energy is therefore large enough, we make the following estimation. The irradiations were performed with 92 MeV $^{129}Xe^{23+}$ ions which, according to SRIM calculations, correspond to the stopping power of $\sim$15 keV nm^{-1}. At the length of the formed grooves this corresponds to a deposition of $1.65 \cdot 10^3$ keV and $3.5 \cdot 10^3$ keV, respectively, thus resulting in an energy deposition of $\sim$180 eV per atom assuming that indeed all energy is eventually transferred from the electronic system into the lattice. This value is far above typical values for chemical bonding. At this point it has to be mentioned that the estimated groove volume is certainly underestimated due to the finite tip size and the rather narrow groove/ditch.

As mentioned before the formation of similar complex ion tracks after SHI irradiation under grazing incidence were found for CaF$_2$ [17]. For this system, calculations based on a 3D two-temperature-model (TTM) have shown that the

groove and hillock formation can be linked to sublimation and melting processes induced by SHI irradiation. As mica has a much more complex atomic structure compared to CaF$_2$, such TTM simulations have not been attempted until now for this material. It is therefore unknown if the formation of similar track structures on mica can be explained alone by sublimation and melting processes. Theoretical investigations are therefore highly desirable.

3.5. Beyond track formation

First etching investigations have shown that a further treatment of irradiated mica samples leads to the formation of well defined elongated pit structures. The irradiated mica samples were etched in diluted HF (4% vol.) for three minutes and afterwards inspected with the AFM. Figure 8 shows a mica surface after
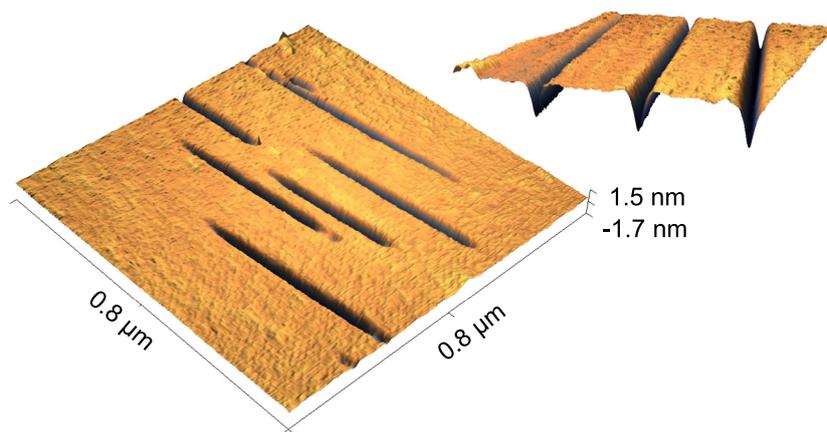
Figure 8. The 92 MeV ^{129}Xe^{23+} irradiated sample were etched in 4% HF etchant solution for three minutes. After etching the tracks appear as parallel arranged elongated pits. The 3D image shows the well defined structure of the elongated pits which exceed at least 1 nm in depth.

92 MeV ^{129}Xe^{23+} irradiation and etching for three minutes. The etching removes all hillocks and leads to a flat surface (RMS-roughness value 0.07 nm) with well-defined parallel-arranged pits only. The pits have a depth of about 1 nm and a width of about ∼30 nm, which corresponds roughly to the width of the double track structure (see figure 6(b)). The topographic features induced by irradiation have been lost after etching.

4. Summary and conclusion

SHI irradiation of muscovite mica under grazing incidence has shown the formation of a complex track structure similar to the one observed recently for CaF$_2$. The created ion track consists of a double track at the impact site which merges into a single protrusion that fades slowly with distance. The length of the track can be controlled by varying the angle of incidence and reaches length of several μm for very shallow incidence angles. Moreover the dimensions of the nanofeatures can be controlled by varying the kinetic energy of the incident ions. The length and the diameter of the double track can be fitted by a square root function of the stopping power with a threshold of ∼4 keV nm^{-1}. Once more it could be shown that the velocity of the incident ion has a decisive influence on the damage production. Detailed studies of the created surface tracks by varying the sample temperature during irradiation have shown only small differences in the created nanostructure features, whereas a change of the chemical composition (muscovite or fluorphlogopite mica) has a noticeable effect on the topography. In the case of fluorphlogopite mica a pronounced groove formation at the impact site could be observed. The lack of bordering nanodots and a comparison of the groove volume with the deposited energy point to the fact that under grazing incidence several thousand of atoms are ejected into vacuum due to the interaction process. Irradiation parameters, like the angle of incidence and the particle kinetic energy, define the total volume and dimensions of the damaged material, which can afterwards be attacked by etching processes. Further etching investigations of irradiated mica under grazing incidence promise the control over the formation of well defined nm-large pit structures and their implementation in lithographic processes.

ORCID iDs

Elisabeth Gruber ● https://orcid.org/0000-0002-1195-3638
Henning Lebius ● https://orcid.org/0000-0002-4347-3073
Marika Schleberger ● https://orcid.org/0000-0002-5785-1186
Friedrich Aumayr ● https://orcid.org/0000-0002-9788-0934

References

[1] Fleischer R L, Price P B and Walker R M 1965 *J. Appl. Phys.* **36** 3645
[2] Toulemonde M, Trautmann C, Balanzat E, Hjort K and Weidinger A 2004 *Nucl. Instrum. Methods* B **216** 1–8
[3] Khalfaoui N, Rotaru C C, Bouffard S, Toulemonde M, Stoquert J P, Haas F, Trautmann C, Jensen J and Dunlop A 2005 *Nucl. Instrum. Methods* B **240** 819–28
[4] Aumayr F, Facsko S, El-Said A S, Trautmann C and Schleberger M 2011 *J. Phys.: Condens. Matter* **23** 393001
[5] Papaleo R, Silva M, Leal R, Grande P, Roth M, Schattat B and Schiwietz G 2008 *Phys. Rev. Lett.* **101** 167601
[6] Akcöltekin E, Peters T, Meyer R, Duvenbeck A, Klusmann M, Monnet I, Lebius H and Schleberger M 2007 *Nat. Nanotechnol.* **2** 290–4
[7] Trautmann C, Schwartz K, Costantini J, Steckenreiter T and Toulemonde M 1998 *Nucl. Instrum. Methods* B **146** 367–78
[8] Toulemonde M, Assmann W, Dufour C, Meftah A and Trautmann C 2012 *Nucl. Instrum. Methods* B **277** 28–39
[9] Ochedowski O, Osmani O, Schade M, Bussmann B K, Ban-d'Etat B, Lebius H and Schleberger M 2014 *Nat. Commun.* **5** 3913
[10] Madauß L, Ochedowski O, Lebius H, Ban-d'Etat B, Naylor C H, Johnson A C, Kotakoski J and Schleberger M 2016 *2D Mater.* **4** 015034
[11] Karlušić M *et al* 2015 *J. Phys. D: Appl. Phys.* **48** 325304

[12] Papaleo R M, Thomaz R, Gutierres L I, de Menezes V M, Severin D, Trautmann C, Tramontina D, Bringa E M and Grande P L 2015 *Phys. Rev. Lett.* **114** 118302

[13] Roll T, Meier M, Akcöltekin S, Klusmann M, Lebius H and Schleberger M 2008 *Phys. Status Solidi* **2** 209–11

[14] Akcöltekin S, Bukowska H, Peters T, Osmani O, Monnet I, Alzaher I, Ban-d'Etat B, Lebius H and Schleberger M 2011 *Appl. Phys. Lett.* **98** 103103

[15] Ochedowski O, Kleine Bussmann B, Ban-d'Etat B, Lebius H and Schleberger M 2013 *Appl. Phys. Lett.* **102** 153103

[16] Ochedowski O, Lehtinen O, Kaiser U, Turchanin A, Ban-d'Etat B, Lebius H, Karlušić M, Jakšić M and Schleberger M 2015 *Nanotechnology* **26** 465302

[17] Gruber E *et al* 2016 *J. Phys.: Condens. Matter* **28** 405001

[18] Lang M, Glasmacher U A, Moine B, Neumann R and Wagner G A 2004 *Nucl. Instrum. Methods* B **218** 466–71

[19] Hagen T, Grafstrom S, Ackermann J, Neumann R, Trautmann C, Vetter J and Angert N 1994 *J. Vac. Sci. Technol.* **12** 1555–8

[20] Thibaudau F, Cousty J, Balanzat E and Bouffard S 1991 *Phys. Rev. Lett.* **67** 1582–5

[21] Ackermann J 1996 *Nucl. Instrum. Methods* B **107** 181–4

[22] Dobeli M, Ames F, Musil C R, Scandella L, Suter M and Synal H A 1998 *Nucl. Instrum. Methods* B **143** 503–12

[23] Daya D B *et al* 1995 *Nucl. Instrum. Methods* B **106** 38–42

[24] Daya D B, Reimann C, Hallén A, Sundqvist B and Håkansson P 1996 *Nucl. Instrum. Methods* B **111** 87

[25] Daya D B, Reimann C, Håkansson P, Sundqvist B, Brunelle A, Della-Negra S and Le Beyec Y 1997 *Nucl. Instrum. Methods* B **124** 484

[26] Nečas D and Klapetek P 2012 *Open Phys.* **10** 181–8

[27] Akcöltekin E, Akcöltekin S, Osmani O, Duvenbeck A, Lebius H and Schleberger M 2008 *New J. Phys.* **10** 053007

[28] Akcöltekin S, Akcöltekin E, Roll T, Lebius H and Schleberger M 2009 *Nucl. Instrum. Methods Phys. Res.* B **267** 1386–9

[29] Toulemonde M, Bouffard S and Studer F 1994 *Nucl. Instrum. Methods Phys. Res.* B **91** 108–23

[30] Ziegler J F, Ziegler M D and Biersack J P 2010 *Nucl. Instrum. Methods* B **268** 1818–23

[31] Bouffard S, Leroy C, Della-Negra S, Brunelle A and Costantini J 2001 *Phil. Mag.* A **81** 2841–54

[32] Ochedowski O, Bussmann B K and Schleberger M 2014 *Sci. Rep.* **4** 6003

[33] Wirth R 1985 *J. Mater. Sci. Lett.* **4** 327–30

[34] Cartz L and Tooper B 1965 *J. Appl. Phys.* **36** 2783–7

[35] Singh M, Kaur N and Singh L 2010 *Radiat. Phys. Chem.* **79** 1180–8